Al-Azhar University Civil Engineering Research Magazine (CERM)
Vol. (44) No. (2) April. 2022

Egyptian Precipitable Water Vapor Study Using Low Earth Orbit Satellite and Reanalysis Data

Abd Elrahman Yassien[2,*], Ashraf El-Kutb Mousa[3], Mostafa Rabah[1], Ahmed Saber[1], Mohamed Zhran[4]

[1]Civil Engineering Department, Benha Faculty of Engineering, Benha University, Benha, Egypt.
[2]Civil Engineering Department, Mansoura Higher Institute for Engineering and Technology, Mansoura, Egypt.
[3]National Research Institute of Astronomy and Geophysics (NRIAG), Helwan, Egypt.
[4]Public Works Engineering Department, Faculty of Engineering, Mansoura University, Mansoura, Egypt.
*Corresponding Author E-mail: abyassin@mc.edu.eg

الملخص عربي:

الدافع الأساسي لتغير المناخ هو الاختلافات في بخار الماء في الغلاف الجوي، وهو عنصر حيوي في التحكم في درجة حرارة الأرض ويلعب دورا مهما في إشعاع الغلاف الجوي العالمي، ودورة المياه، وتأثير توازن الطاقة. لذلك، تهدف هذه الدراسة إلى اكتشاف التباين الزماني المكاني لبخار الماء القابل للهبوط (PWV) في المنطقة المصرية باستخدام بيانات المدار الأرضي المنخفض (LEO) وبيانات إعادة التحليل. قيم PWV بواسطة LEO أو بيانات إعادة التحليل لها اتجاهات مماثلة بشكل عام. يبدو أن PWV يحتوي على نمط عرضي تكون فيه علاقته علاقة عكسية. ترتبط خطوط العرض الأعلى بقيم PWV الأكبر، بينما ترتبط خطوط العرض الأدنى بقيم أقل. يوجد زيادة العديد بقيم الـ PWV في مواقع قريبة من ساحل البحر الأبيض المتوسط. العلاقة بين PWV وخط الطول غير واضحة. وبالتالي يتأثر PWV في الغالب بخط العرض. يحدث زيادة بعض قيم الـ PWV في مواقع قريبة من ساحل البحر الأحمر. خلال مدة الدراسة وهي 16 عاما من 2006 إلى 2021، بلغ الحد الأقصى لمتوسطPWV السنوي عبر المنطقة المصرية 14.72 ملم في 2018 بواسطة LEO و19.24 ملم في 2015 بواسطة بيانات إعادة التحليل. أكبر متوسط موسمي لـ PWV هو 22.67 ملم في صيف 2019 بواسطة LEO وببيانات إعادة التحليل هو 29 ملم في صيف 2019. الحد الأدنى لمتوسط موسمي لـ PWVهو 9.15 ملم في شتاء 2008 بواسطة LEO وبواسطة بيانات إعادة التحليل هو 12.71 ملم في شتاء 2017. كانت قيم PWV هي الأعلى في أغسطس، وبالتحديد أغسطس 2019 عند حوالي 24 ملم بواسطة LEO وبحسب بيانات إعادة التحليل هي 31.49 ملم في أغسطس 2019. أدنى قيم PWV كانت في يناير 2015 عند حوالي 7.67 ملم بواسطة المدار الأرضي المنخفض وببيانات إعادة التحليل هي 11.48 ملم في يناير 2015. في بحثنا، كانت قيم PWV بواسطة بيانات إعادة التحليل أعلى من نظيراتها من LEO PWV لأن ملفات RO لديها تقريبا أدنى ارتفاع في نقطة الحضيض أكثر من ملفات بيانات إعادة التحليل التي قد تؤدي إلى نتائج أقل من القيم الحقيقية لأن PWV أعلى عند الارتفاعات المنخفضة. لذلك، يوصى بإجراء دراسة عميقة لتحسين نتائج PWV بواسطة.LEO

Abstract :

The fundamental driver of climate change is variations in atmospheric water vapor, which is a vital component in controlling Earth's temperature and plays a significant role in global atmospheric radiation, water cycle, and energy balance effect. So, this study aims to discover at the spatiotemporal variation of Precipitable Water Vapor (PWV) in the Egyptian region using Low Earth Orbit (LEO) and reanalysis data. The retrieval PWV by LEO or reanalysis data has similar trends overall. The PWV seems to have a latitudinal pattern in which its relationship to latitude is inverse. Higher latitudes are correlated with bigger PWV values, whereas lower latitudes are correlated with lower values. Many PWVs are increased at locations close to the coast of the Mediterranean Sea. Relationship between PWV and longitude is not clear. PWV is thus mostly influenced by latitude. Some PWVs are increased at locations close to the coast of the red Sea. During the 16-year research period from 2006 to 2021, the maximum annual averaged PWV across Egyptian region is 14.72 millimeters in 2018 by LEO and 19.24 millimeters in 2015 by reanalysis data. The greatest seasonal averaged PWV is 22.67 millimeters in summer 2019 by LEO and by reanalysis data is 29 millimeters in summer 2019. The minimum seasonal averaged for PWV is 9.15 millimeters in winter 2008 by LEO and by ERA-Interim is 12.71 millimeters in winter 2017. PWV values are highest in August, precisely August 2019 at approximately 24 millimeters by LEO and by reanalysis data are 31.49 millimeters in August 2019. lowest PWV values are in January 2015 at around 7.67 millimeters by LEO and by reanalysis data are 11.48 millimeters in January 2015. In our research, PWV values by reanalysis are higher than corresponding LEO PWVs because the RO profiles almost have the lowest perigee height more than the reanalysis data profiles which might result in lower PWV results than the true values because PWV is higher at lower altitudes. So, it is recommended to make a deep study to improve the PWV results by LEO.

Keywords: Precipitable water vapor; Radio occultation; GNSS.

1. INTRODUCTION

The fundamental driver of climate change is variations in atmospheric water vapor, which is a vital component in controlling Earth's temperature and plays a significant role in global atmospheric radiation, water cycle, and energy balance effect [1]. Precipitable Water Vapor (PWV) is the term used to describe the total amount of water vapor in an atmosphere's vertical column per unit area. For the development of weather and climate prediction, it is essential to comprehend the spatiotemporal variability of water vapor.

Several methods and platforms are currently available to detect atmospheric PWV; in general, there are two types of devices or sensors: ground-based and space-based. PWV can be found using ground-based techniques like solar photometry and radiosonde (RS). On the other hand, space-based observational techniques include radio occultation (RO), the Moderate Resolution Imaging Spectroradiometer (MODIS), and the Atmospheric Infrared Sounder (AIRS).

Due to their poor, non-uniform geographic distribution and constrained temporal obtainability, ground-based techniques like RS fall short in capturing the ongoing changes in PWV. The RS, however, is a useful reference device for atmospheric sounding [2]. Although ground-based GNSS technology has several advantages, it is recognized as a trustworthy instrument for tracking PWV change in real-time. It has the capacity to continually monitor and perceive [3]. GNSS stations have a limited spatial resolution, especially in the water, according to those run by the International GNSS Service (IGS). In other instances, more conventional PWV estimating techniques, such as solar photometry and microwave radiometry, are used. Due to cost and observing situation restrictions, these sensors can't be utilized widely, and it's challenging to compile a consistent and varied collection of observations.

In the latest decades, climatic parameters and PWV dispersion have been detected from space using techniques like RO and microwave satellite-borne passive microwave detectors [4]. They offer some advantages over alternative methods. In particular, RO's data are unaffected by clouds and precipitation and have a high vertical resolution [5]; Additionally, it has a global observation coverage that is not restricted by land, the ocean, or the sea, therefore RO is used to compute PWV around the world in all-weather circumstances [6].

1.1. GNSS Radio Occultation

A GNSS receiver on a Low Earth Orbit (LEO) satellite may detect signals given by GNSS satellites as they pass through the Earth's atmosphere using the active limb sounding technique known as Radio Occultation (RO) in the Global Navigation Satellite System (GNSS) as presented in **Fig. 1**. Since the phase measurements are based on time measurements using very precise clocks aboard the GNSS and LEO satellites, RO measurements are long-term stable and do not require satellite-to-satellite inter-calibration [7].

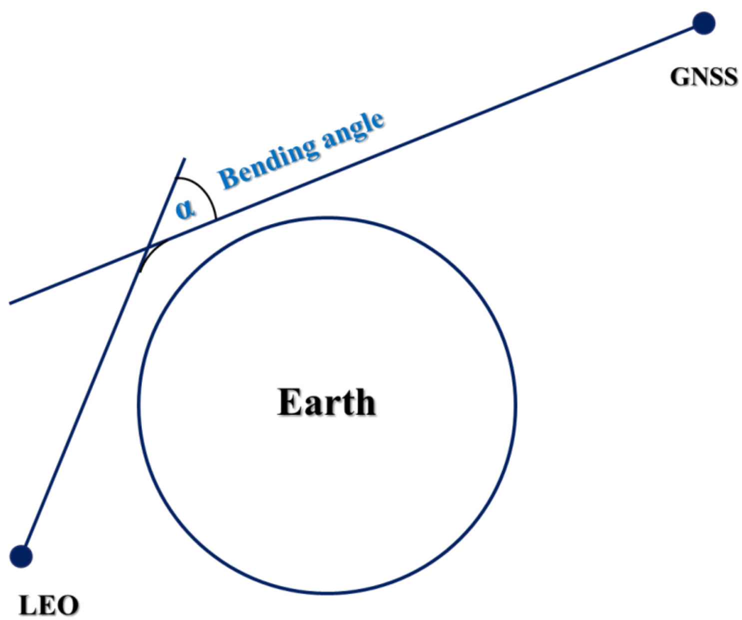

Fig. 1: Geometry of GNSS – LEO satellite occultation.

The interaction between electromagnetic radiation and the atmosphere employing limb-sounding geometry is the fundamental tenet of the RO approach. The refractive field of the

Earth causes a ray to be twisted and delayed as it travels through the atmosphere. Total bending angle, which is a function of the impact parameter, may be used to describe the atmosphere's overall influence [8].

A GNSS RO event happens while a GNSS satellite is rising behind the Earth's limb as observed by a GNSS receiver aboard a LEO satellite. The Earth's atmosphere causes a delay in the signals that GNSS satellites relay to LEO satellites. By using a series of transformation processes, this delay may be precisely measured, transformed into a vertical profile of bending angles, and then processed to obtain a refractivity profile [9].

1.2. Numerical Weather Perdition Reanalysis Data

The reanalysis data was created using a variety of models, including ERA-15, ERA-40, ERA-Interim, and ERA5. It was created in the 1980s. A numerical weather prediction model run by the European Centre for Medium-Range Weather Forecasting (ECMWF) from 1979 to the present produced the global atmospheric reanalysis data collection known as ERA-Interim. ERA-Interim has a spatial resolution of 79 kilometers (0.75°×0.75°) and a temporal resolution of 6 hours [10]. ERA-Interim is a world reanalysis dataset that applies the 4D-Var method to depict the atmospheric status [11] and assimilates various observations such as RS humidity, atmospheric Infrared Sounder (AIRS), GNSS RO bending angle profiles, and Special Sensor Microwave/Imager (SSM/I), European Remote Sensing (ERS-1 and -2 [10].

Previous research on the reliability of GNSS RO and radiosonde recovered PWV has shown the usefulness of these observations for weather and climate studies. PWV generally exhibits seasonal and latitudinal variations. About the equator, the average PWV is at its highest, hovering around 40 millimeters, before falling to 10 millimeters in the polar region. When the temperature is warmer and colder in both hemispheres, PWV levels are greater and lower, respectively. The surface temperature and the water vapor supply are shown to be closely related to regional and seasonal fluctuations in PWV [12].

Using radio occultation measurements for sixteen years, the main objective of this work is to provide an initial analysis of the geographical and temporal fluctuations in PWV over Egypt in recent decades. The study area and methodology of the obtained data are both covered in Section 2. Section 3 presents the variations of PWV changes over the Egyptian area. Finally, Section 4 illustrates the conclusions and suggestions for future research.

2. METHODOLOGY

2.1. Research region

The research region is the Egyptian area which is situated between latitudes 22◦ and 32◦ North and longitudes 24◦ and 37◦ East. In our research, the collected data over Egypt has an extensive-ranging of latitude-longitude differences ±5°/±5°.

2.2. Data collection

The Constellation Observing System for Meteorology, Ionosphere, and Climate (COSMIC) RO soundings from a satellite-based global navigation satellite system supply the meteorological data for atmospheric wet profiles across the world. The phase delay of radio signals from satellites when they are obscured by the Earth's atmosphere is seen by the COSMIC spacecraft' GNSS radio occultation sensors. Calculating atmospheric refractivity profiles may be done using the signal bending angles in various atmospheric layers. The COSMIC Data Analysis and Archive Center provided temperature, pressure, and refractivity profiles to the GNSS RO (CDAAC). With a vertical height resolution of around fifty meters for COSMIC-2, it includes over five thousands daily profiles scattered throughout the globe, each of which is longer than 40 km. on the other hand, the COSMIC-1 archive has about one thousand atmospheric profiles with a vertical height resolution of around one hundred meters.

The CDAAC website provides RO datasets for COSMIC-1 and COSMIC-2 (https://cdaac-www.cosmic.ucar.edu/cdaac/index.html). Sixteen years of datasets of COSMIC-1 and COSMIC-2 were downloaded from the CDAAC website and reduced for the Egyptian region analysis. COSMIC-1 datasets are from April 2006 to April 2020 about 14 years datasets and COSMIC-2 are from October 2019 to June 2021. Also, the ERA-Interim temperature, pressure, and moisture profiles are available through the CDAAC website. The ECMWF gridded analysis produced these profiles, which were spatially and temporally interpolated with RO events.

Fig. 2 represents the COSMIC-2 RO events distribution between 2019 and 2021 in the Egyptian region. **Fig. 3** describes the COSMIC-1 RO events distribution between 2006 and 2020 in the Egyptian region. **Fig. 4** demonstrates the COSMIC-1 and COSMIC-2 RO events distribution for the research period in the Egyptian region. **Fig. 5** shows the COSMIC-1 RO events distribution in 2007 in the Egyptian region as a year sample.

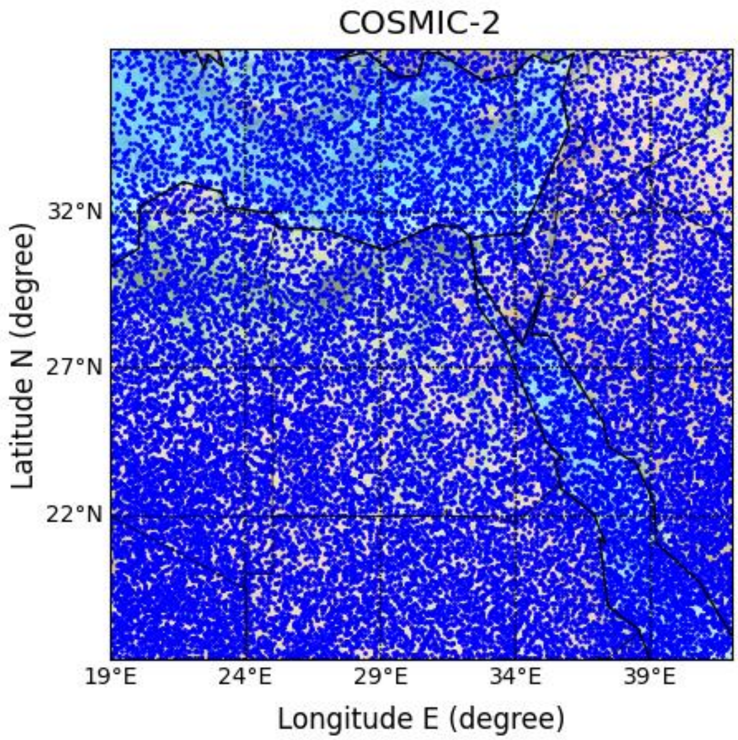

Fig. 2: COSMIC-2 RO events distribution 2019 and 2021 in the Egyptian region.

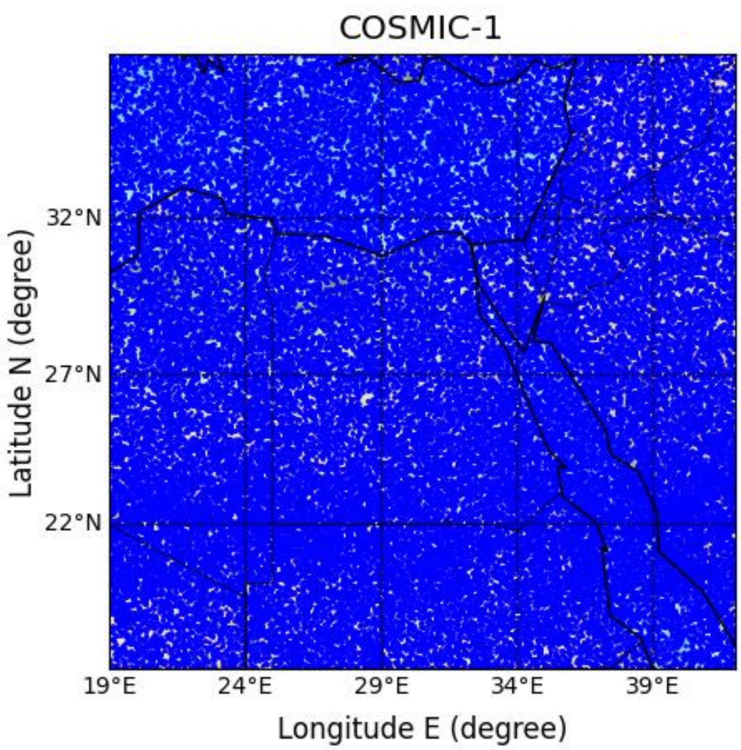

Fig. 3: COSMIC-1 RO events distribution 2006 and 2020 in the Egyptian region.

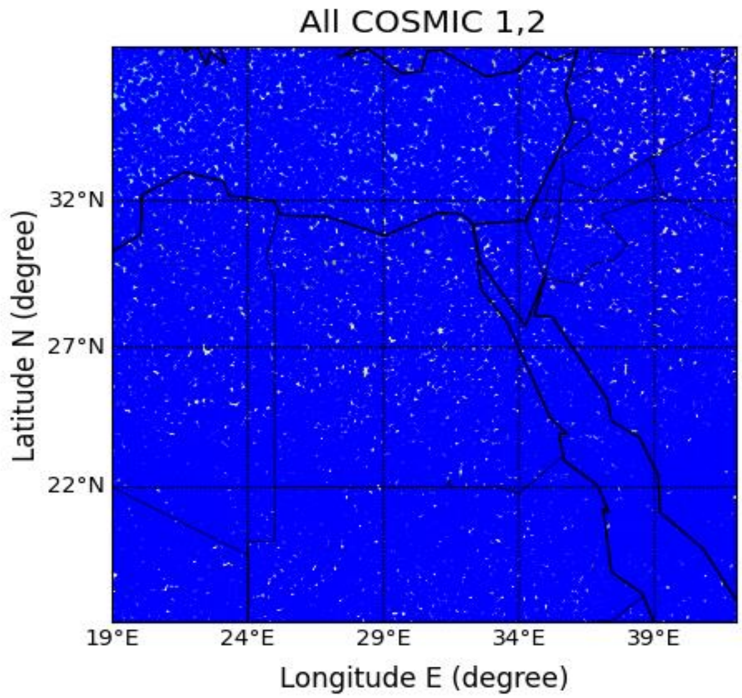

Fig. 4: COSMIC-1 and COSMIC-2 RO events distribution for the research period in the Egyptian region.

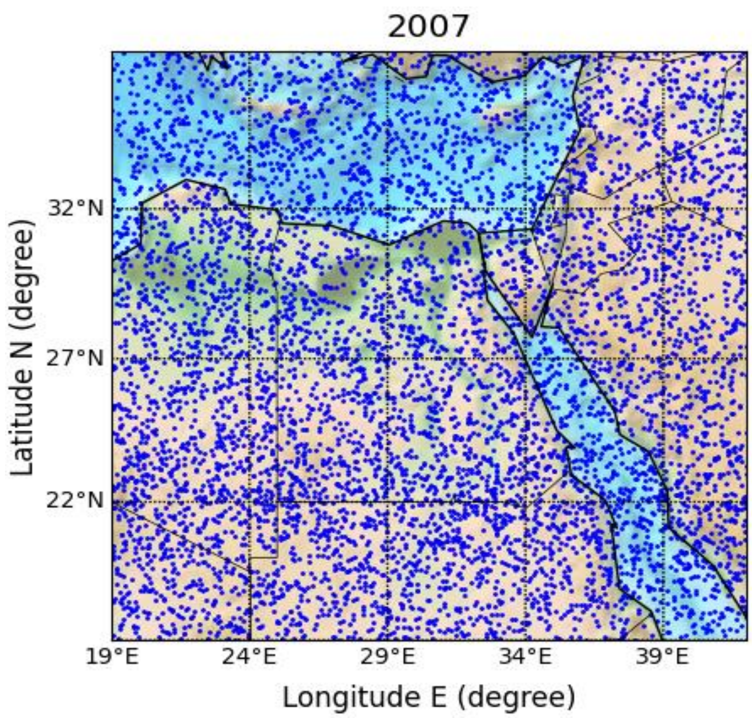

Fig. 5: COSMIC-1 RO events distribution in 2007 in the Egyptian region.

Table 1 displays the number of COSMIC-1 and COSMIC-2 RO events between April 2006 to June 2021 in the research area.

Table 1: Number of COSMIC-1 and COSMIC-2 RO events between April 2006 to June 2021 in the research area

6	**Year**	**7**	**COSMIC-1**	**8**	**COSMIC-2**
9	2006	**10**	2422	**11**	-
12	2007	**13**	6800	**14**	-
15	2008	**16**	6746	**17**	-
18	2009	**19**	6921	**20**	-
21	2010	**22**	5306	**23**	-
24	2011	**25**	4643	**26**	-
27	2012	**28**	4767	**29**	-
30	2013	**31**	5601	**32**	-
33	2014	**34**	4211	**35**	-
36	2015	**37**	3956	**38**	-
39	2016	**40**	2646	**41**	-
42	2017	**43**	1416	**44**	-
45	2018	**46**	894	**47**	-
48	2019	**49**	411	**50**	2739
51	2020	**52**	2	**53**	15580
54	2021	**55**	-	**56**	7918

2.2.1. Data analysis

The processed RO data may be utilized to generate atmospheric refractivity (N) based on the bending angles under the spherical symmetry assumption (Kursinski et al., 2000). Refractivity in the upper and intermediate troposphere has a major role in determining temperature. The primary application of refractivity information is to extract water vapor since atmospheric refractivity is more closely connected to changes in water vapor than to changes in temperature, especially at the lowest tropospheric heights [14]. Teng et al. (2013) propose that Equation 1 could be used to calculate the water vapor pressure.

$$N = 77.6\frac{P}{T} + 3.73\times10^{5}\frac{e}{T^{2}} \tag{1}$$

Where N is the refractivity, T is the temperature in Kelvins, P is the air pressure in hectopascal, and e is the water vapor pressure in hectopascal:

The specific humidity (q) could be calculated based on water vapor and air pressure [15], and Equation 2 displays how to calculate the specific humidity

$$q = \frac{\varepsilon e}{P - (1-\varepsilon)e} \tag{2}$$

Where ε is a constant ($\varepsilon = 0.622 g.kg^{-1}$)

The PWV value of one wet profile is computed by integration of the specific humidity with the heights, and Equation 3 presents this definite integral.

$$w = \frac{1}{\rho g}\int_{0}^{P_s} q dp = -\frac{1}{g}\sum_{Ps}^{0} q \Delta P \tag{3}$$

Where W denotes the PWV value in millimeters, ρ is the liquid water density, P is air pressure, Ps is the surface air pressure, and g is the gravitational acceleration value.

Negative refractivity might result from the super-refraction in the lower tropospheric altitudes [16], which leads to humidity biases and void data from zero altitude to the minimum altitude. Profiles having the lowest perigee height of more than 500 meters were excluded from this analysis because PWV is higher at lower altitudes. The collected GNSS RO profiles datasets from the CDAAC service were analyzed. **Fig. 6** and **Fig. 7** summarize the COSMIC-1 and COSMIC-2 datasets process.

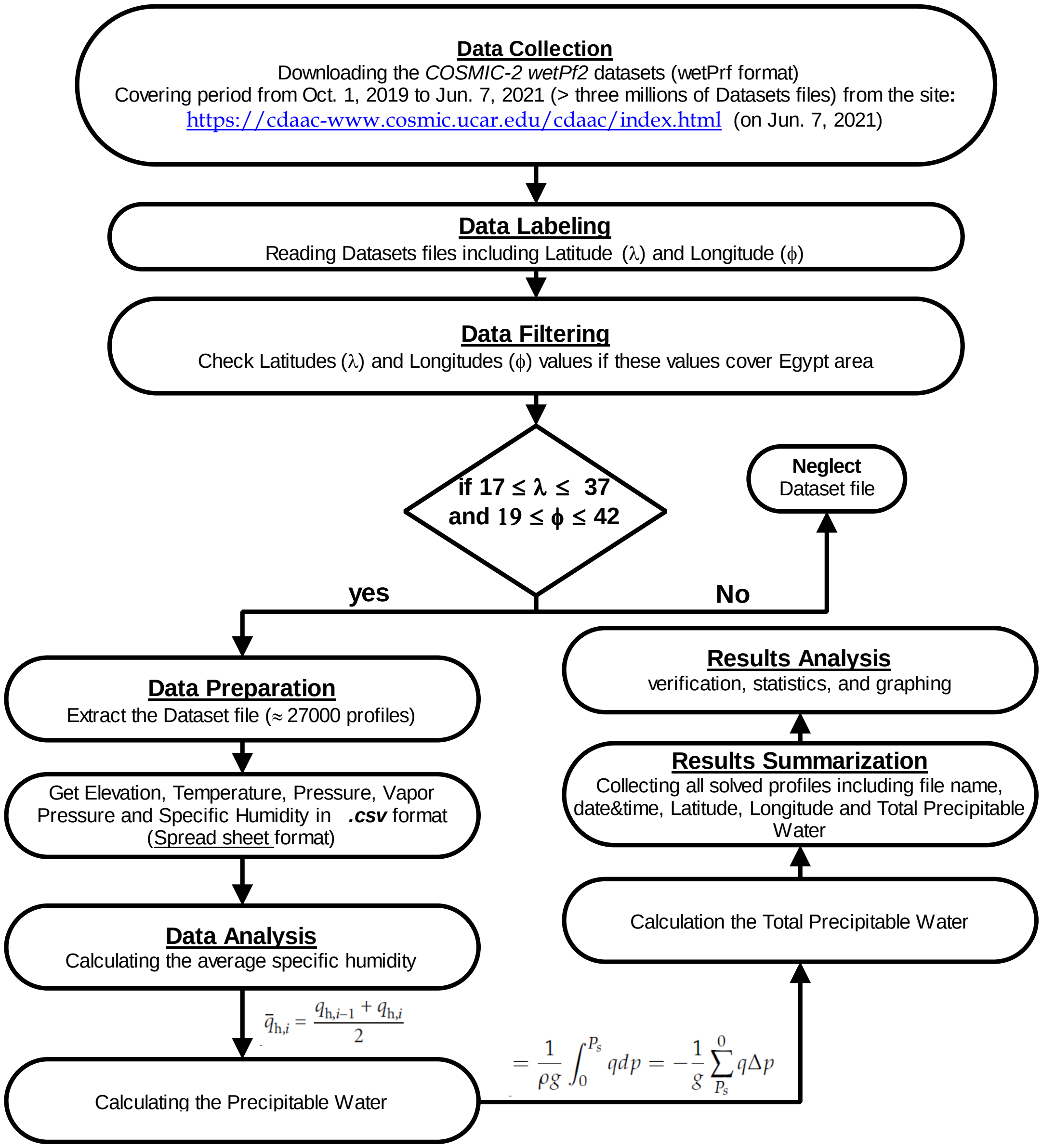

Fig. 6: COSMIC-2 GNSS RO profiles analysis process.

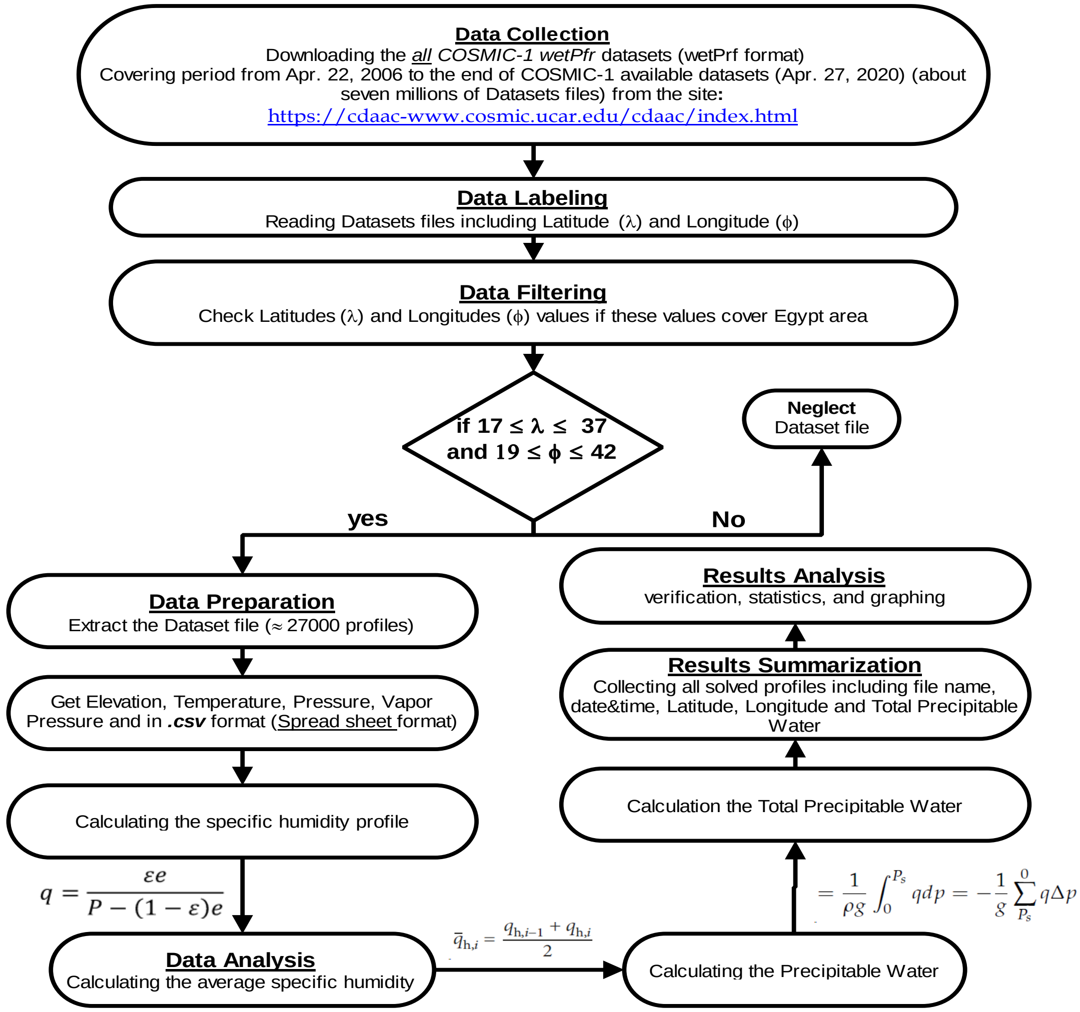

Fig. 7: COSMIC-1 GNSS RO profiles analysis process.

Also, we download the ERA-Interim moisture profiles through the CDAAC service for the study period between April 2006 and June 2021 and we also calculate the PWV using the integral Equation 3.

3. RESULTS AND DISCUSSIONS

We divide this section into two primary sections: spatial variability and temporal variability.

3.1. Spatial Variability

3.1.1. PWV with Latitude

The research area is stripped latitudinally and each strip is one degree of latitude then the averaged PWV values are computed at each strip. **Fig. 8 and Fig. 9** illustrate the relation between PWV and latitude for COSMIC-2 and COSMIC-1 respectively. overall, it clear that an inverse relationship between PWV and latitude. Therefore, it is clear that lower latitudes have increased PWV. The retrieval PWV by LEO or ERA-Interim often demonstrates similar trends

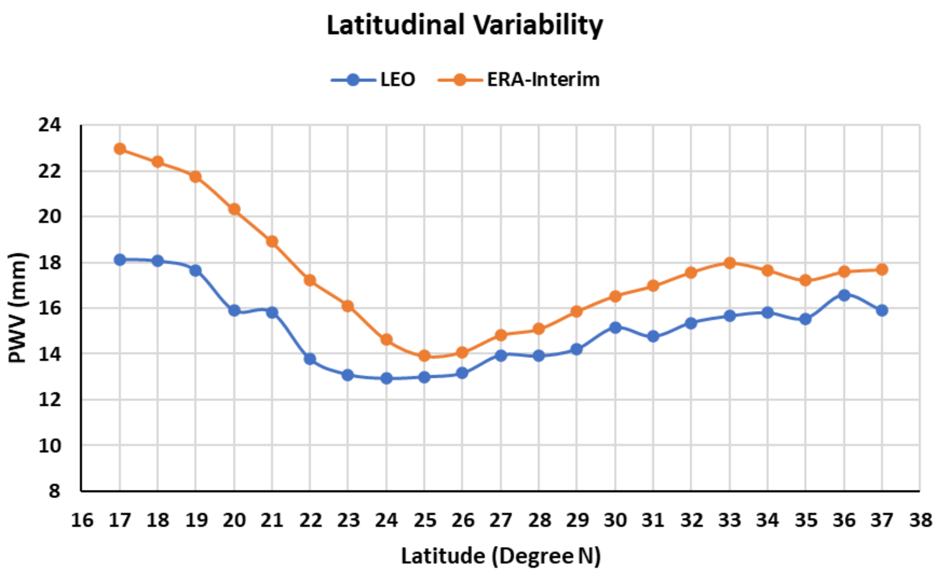

Fig. 8: PWV variability with latitudes COSMIC-2 and ERA-Interim

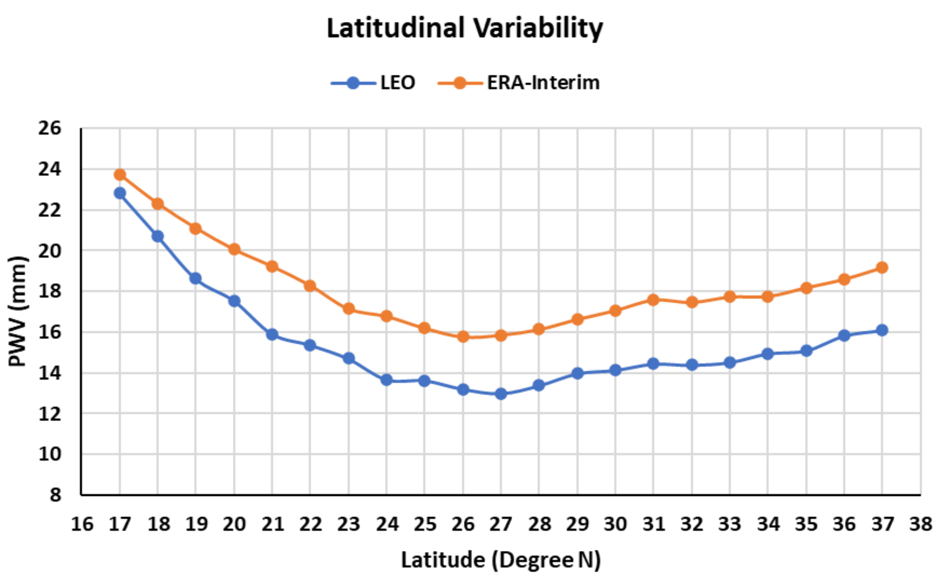

Fig. 9: PWV variability with latitudes COSMIC-1 and ERA-Interim

The PWV seems to have a latitudinal pattern in which its relationship to latitude is inverse. Higher latitudes are correlated with bigger PWV values, whereas lower latitudes are correlated with lower values. Many PWVs are increased at locations close to the coast of the Mediterranean Sea.

3.1.2. PWV with Longitude

As in the previous section, the research area is stripped longitudinally and each strip is one degree of longitude then the averaged PWV values are computed at each strip. **Fig. 10 and Fig. 11** illustrate the relation between PWV and longitude for COSMIC-2 and COSMIC-1 respectively. Generally, relationship between PWV and longitude is not clear. PWV is thus mostly influenced by latitude. Some PWVs are increased at locations close to the coast of the red Sea. Also, the retrieval PWV by LEO or ERA-Interim has similar trends overall.

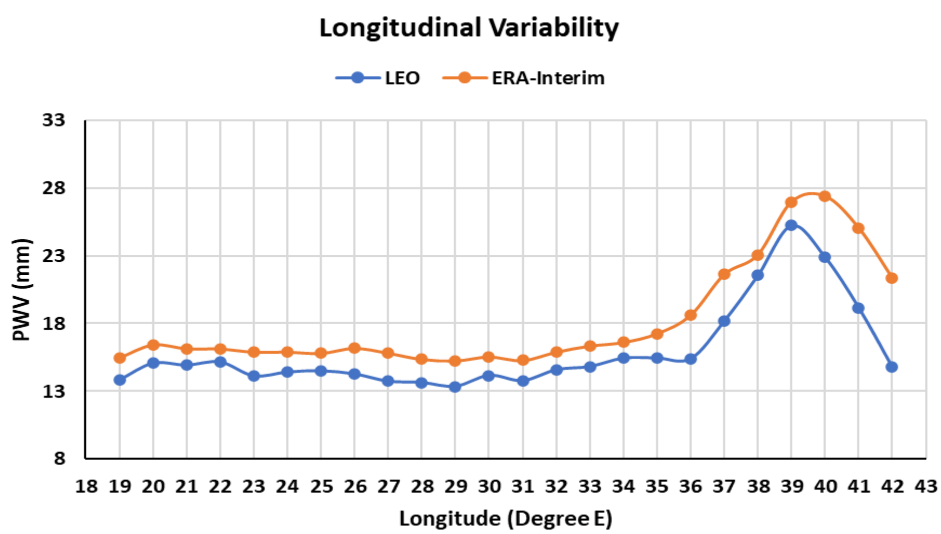

Fig. 10: PWV variability with longitudes COSMIC-2 and ERA-Interim

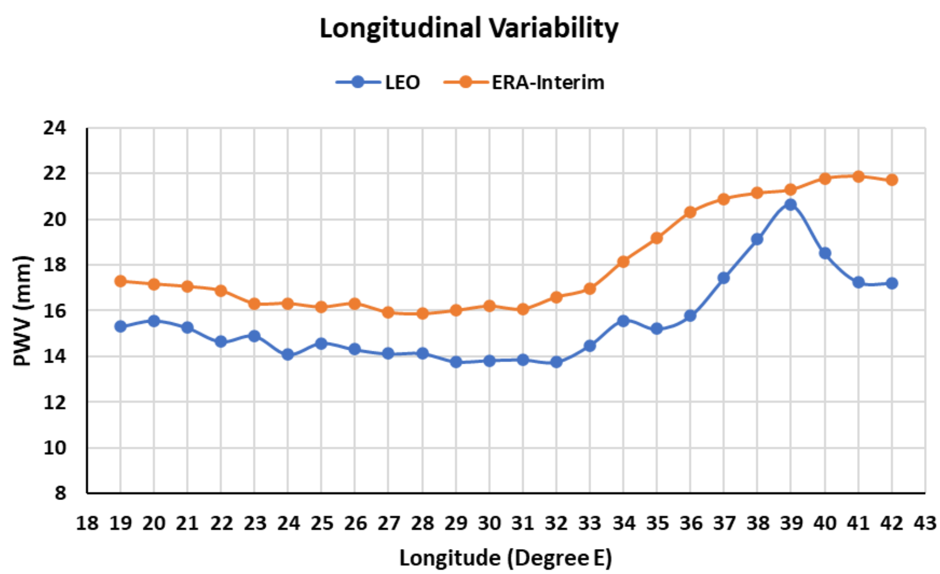

Fig. 11: PWV variability with longitudes COSMIC-1 and ERA-Interim

3.2. Temporal Variability

PWV Temporal variability is separated into three sections: variability with years, variability with seasons, and variability with months. It should be emphasized that just the Egyptian region was used for the statistical analysis, which was located from 22◦ to 31◦ 36' N of latitudes and from 24◦ to 37◦ E of longitudes.

3.2.1. PWV variability with Years

The mean PWV is computed at each year from the LEO and ERA-Interim. **Fig. 12** presents the averaged PWV of the research area at each year using LEO and ERA-Interim.

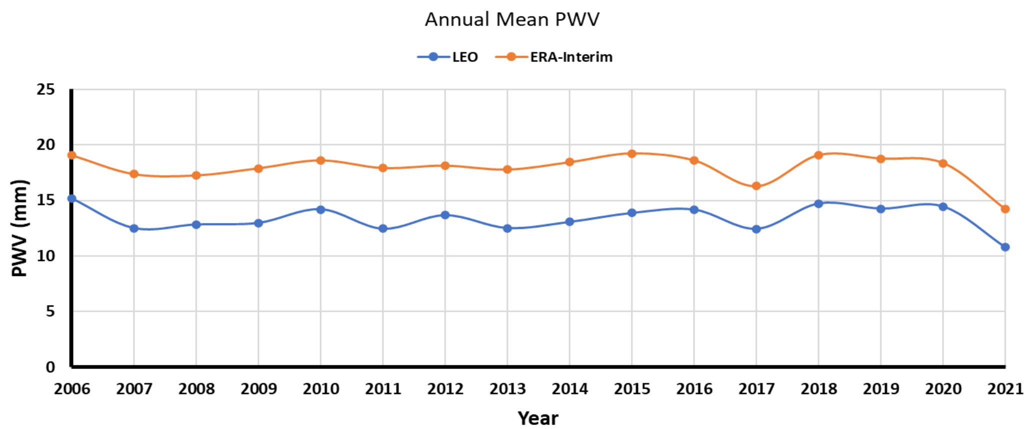

Fig. 12: The averaged PWV of the research area at each year using LEO and ERA-Interim

The averaged PWV values of the Egyptian region are between 10.78 millimeters to 15.19 millimeters using LEO and by ERA-Interim ranges from 14.21 millimeters to 19.24 millimeters.

3.2.2. PWV variability with Seasons

Every year is divided into four three-month seasons to analyze the seasonal fluctuation of PWV: December–January–February (DJF, in short; winter), June–July–August (JJA, in short; summer), March–April–May (MAM, in short; spring), and September–October–November (SOM, in short; autumn) (SON, in short; autumn). The seasonal averaged PWV of the Egyptian region is displayed in **Fig. 13**.

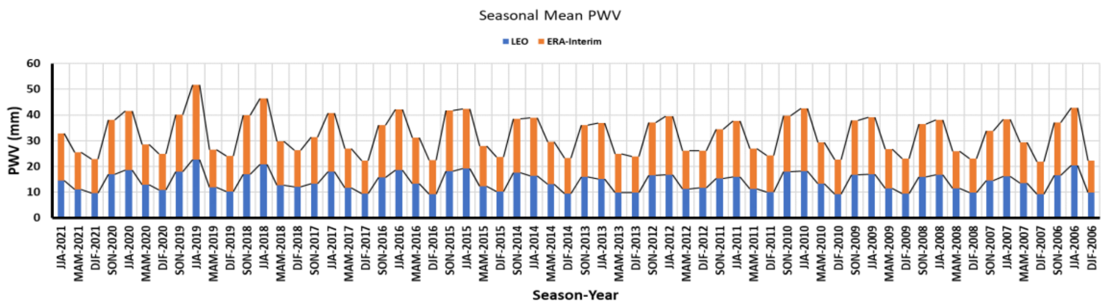

Fig. 13: The averaged PWV of the research area at each season using LEO and ERA-Interim

According to **Fig. 13**, PWVs are greater during the summer between 14.49 millimeters and 22.67 millimeters by LEO and by ERA-Interim range from 18.39 millimeters to 29 millimeters. The lower PWVs are during the winter between 9.15 millimeters and 12.17 millimeters by LEO and by ERA-Interim range from 12.22 millimeters to 14.42 millimeters.

3.2.3. PWV variability with Months

Fig. 14 presents the averaged PWVs at every month over Egyptian region.

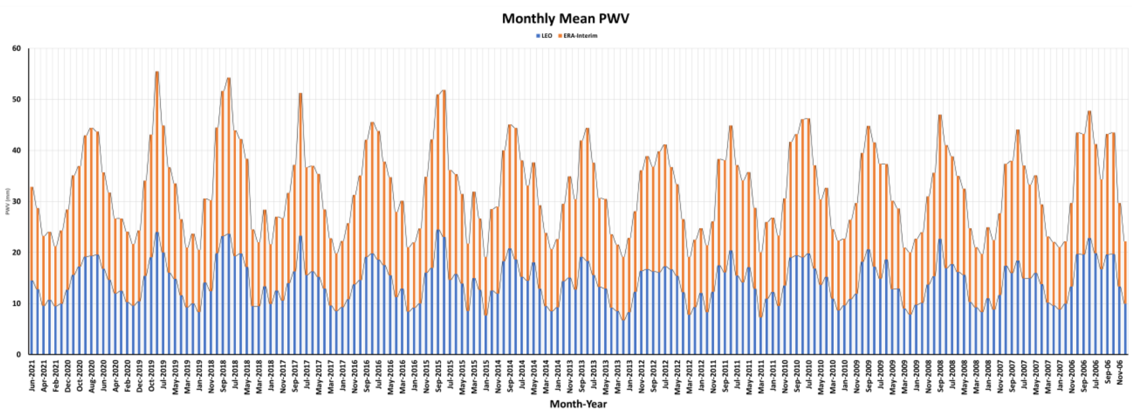

Fig. 14: The averaged monthly PWV of the research area using LEO and ERA-Interim

PWV levels range from 16.12 millimeters to 24 millimeters by LEO by ERA-Interim range from 23.69 millimeters to 31.49 millimeters in August, which is the highest month According to **Fig. 14**. the lowest PWVs, which range from 7.67 millimeters to 24.27 millimeters by LEO by ERA-Interim range from 11.47 millimeters to 14.55 millimeters in January.

57 SUMMARY AND CONCLUSIONS

This study aims to discover at the spatiotemporal variation of PWV in the Egyptian region, and the following conclusions can be summarized:

1) The retrieval PWV by LEO or ERA-Interim has similar trends overall.

2) The PWV seems to have a latitudinal pattern in which its relationship to latitude is inverse.

Higher latitudes are correlated with bigger PWV values, whereas lower latitudes are correlated with lower values. Many PWVs are increased at locations close to the coast of the Mediterranean Sea. Relationship between PWV and longitude is not clear. PWV is thus mostly influenced by latitude. Some PWVs are increased at locations close to the coast of the red Sea.

3) Additionally, during the 16-year research period from 2006 to 2021, the maximum annual averaged PWV across Egyptian region is 14.72 millimeters in 2018 by LEO and 19.24 millimeters in 2015 by ERA-Interim.

4) The greatest seasonal averaged PWV is 22.67 millimeters in summer 2019 by LEO and by ERA-Interim is 29 millimeters in summer 2019. The minimum seasonal averaged for PWV is 9.15 millimeters in winter 2008 by LEO and by ERA-Interim is 12.71 millimeters in winter 2017.

5) PWV values are highest in August, precisely August 2019 at approximately 24 millimeters by LEO and by ERA-Interim are 31.49 millimeters in August 2019. lowest PWV values are in January 2015 at around 7.67 millimeters by LEO and by ERA-Interim are 11.48 millimeters in January 2015.

6) In our research, PWV values by ERA-Interim are higher than corresponding LEO PWVs because the RO profiles almost have the lowest perigee height more than the ERA-Interim profiles which might result in lower PWV results than the true values because PWV is higher at lower altitudes. So, it is recommended to make a deep study to improve the PWV results by LEO.

58 REFERENCES

[1] A. Al-Mashagbah and M. Al-Farajat, "Assessment of Spatial and Temporal Variability of Rainfall Data Using Kriging, Mann Kendall Test and the Sen?s Slope Estimates in Jordan from 1980 to 2007," *Res. J. Environ. Earth Sci.*, vol. 5, no. 10, pp. 611–618, 2013, doi: 10.19026/rjees.5.5691.

[2] S. Gong, D. F. T. Hagan, X. Wu, and G. Wang, "Spatio-temporal analysis of precipitable water vapour over northwest China utilizing MERSI/FY-3A products," *Int. J. Remote Sens.*, vol. 39, no. 10, pp. 3094–3110, May 2018, doi: 10.1080/01431161.2018.1437298.

[3] Z. Dong and S. Jin, "3-D Water Vapor Tomography in Wuhan from GPS, BDS and GLONASS Observations," *Remote Sens. 2018, Vol. 10, Page 62*, vol. 10, no. 1, p. 62, Jan. 2018, doi: 10.3390/RS10010062.

[4] C. A. Mears, J. Wang, D. Smith, and F. J. Wentz, "Intercomparison of total precipitable water measurements made by satellite-borne microwave radiometers and ground-based GPS instruments," *J. Geophys. Res.*, vol. 120, no. 6, pp. 2492–2504, 2015, doi: 10.1002/2014JD022694.

[5] S. P. Ho, L. Peng, C. Mears, and R. A. Anthes, "Comparison of global observations and trends of total precipitable water derived from microwave radiometers and COSMIC

radio occultation from 2006 to 2013," *Atmos. Chem. Phys.*, vol. 18, no. 1, pp. 259–274, 2018, doi: 10.5194/acp-18-259-2018.

[6] X. Meng, J. Cheng, and S. Liang, "Estimating Land Surface Temperature from Feng Yun-3C/MERSI Data Using a New Land Surface Emissivity Scheme," *Remote Sens. 2017, Vol. 9, Page 1247*, vol. 9, no. 12, p. 1247, Dec. 2017, doi: 10.3390/RS9121247.

[7] U. Foelsche, B. Scherllin-Pirscher, F. Ladstädter, A. K. Steiner, and G. Kirchengast, "Refractivity and temperature climate records from multiple radio occultation satellites consistent within 0.05%," *Atmos. Meas. Tech.*, vol. 4, no. 9, pp. 2007–2018, 2011, doi: 10.5194/amt-4-2007-2011.

[8] STEINER A., "High resolution sounding of key climate variables using the radio occultation technique," *Diss. Inst. Meteorol. Geophys. Univ. Graz*, 1998, Accessed: Jun. 21, 2022. [Online]. Available: https://cir.nii.ac.jp/crid/1572824500085676800.bib?lang=en

[9] C. Rocken, T. Van Hove, and R. Ware, "Near real-time GPS sensing of atmospheric water vapor," *Geophys. Res. Lett.*, vol. 24, no. 24, pp. 3221–3224, Dec. 1997, doi: https://doi.org/10.1029/97GL03312.

[10] P. Poli, J. Joiner, and E. R. Kursinski, "1DVAR analysis of temperature and humidity using GPS radio occultation refractivity data," *J. Geophys. Res. Atmos.*, vol. 107, no. D20, p. ACL 14-1, Oct. 2002, doi: 10.1029/2001JD000935.

[11] W. H. Teng, C. Y. Huang, S. P. Ho, Y. H. Kuo, and X. J. Zhou, "Characteristics of global precipitable water in ENSO events revealed by COSMIC measurements," *J. Geophys. Res. Atmos.*, vol. 118, no. 15, pp. 8411–8425, 2013, doi: 10.1002/jgrd.50371.

[12] Q. Zhang, J. Ye, S. Zhang, and F. Han, "Precipitable water vapor retrieval and analysis by multiple data sources: Ground-based GNSS, radio occultation, radiosonde, microwave satellite, and NWP reanalysis data," *J. Sensors*, vol. 2018, 2018, doi: 10.1155/2018/3428303.

[13] R. Kursinski, G. Hajj, S. Leroy, and L. Herman, "The GPS Radio Occultation Technique," *Terr. Atmos. Ocean. Sci. J.*, vol. 11, no. 1, 2000, doi: 10.3319/TAO.2000.11.1.53(COSMIC).

[14] S. P. Ho, Y. H. Kuo, and S. Sokolovskiy, "Improvement of the temperature and moisture retrievals in the lower troposphere using AIRS and GPS radio occultation measurements," *J. Atmos. Ocean. Technol.*, vol. 24, no. 10, pp. 1726–1739, 2007, doi: 10.1175/JTECH2071.1.

[15] J. Wang and L. Zhang, "Systematic errors in global radiosonde precipitable water data from comparisons with groud-based GPS measurements," *J. Clim.*, vol. 21, no. 10, pp. 2218–2238, 2008, doi: 10.1175/2007JCLI1944.1.

[16] F. Xie, D. L. Wu, C. O. Ao, E. R. Kursinski, A. J. Mannucci, and S. Syndergaard, "Super-refraction effects on GPS radio occultation refractivity in marine boundary layers," *Geophys. Res. Lett.*, vol. 37, no. 11, 2010, doi: 10.1029/2010GL043299.